Journal of the Meteorological Society of Japan

The DOI for this manuscript is
DOI:10.2151/jmsj.2023-026
J-STAGE Advance published date: August 23rd, 2023
The final manuscript after publication will replace the preliminary version at the above DOI once it is available.

Influence of the stratospheric QBO on seasonal migration of the convective center across the Maritime Continent

Kunihiko Kodera[1]

Meteorological Research Institute
Tsukuba, 305-0052, Japan

Tomoe Nasuno

JAMSTEC, Yokohama, 236-0001, Japan

Seok-Woo Son

School of Earth and Environmental Sciences,
Seoul National University, Seoul, 08826, South Korea

Nawo Eguchi

Research Institute for Applied Mechanics
Kyushu University, Kasuga, 816-8580, Japan

and

Yayoi Harada

Meteorological Research Institute
Tsukuba, 305-0052, Japan

24 Jul 2023

1) Corresponding author: Kunihiko Kodera, Meteorological Research Institute, Tsukuba, JAPAN.
Email: kodera.kk@gmail.com

Abstract

Modulation of tropical convection by the stratospheric quasi-biennial oscillation (QBO) during the Austral summer has become evident in recent studies. In this study, we show that the QBO affects the seasonal migration of the tropical convection from the equatorial Indian Ocean to the Western Pacific: large-scale convection over the Maritime Continent (MC) and western Pacific strengthens and moves eastward more effectively during easterly QBO (QBO–E) austral summers than during westerly QBO counterparts. This relationship is consistent with an enhanced Madden–Julian Oscillation (MJO) in the QBO–E. The monsoonal active convection over the Sumatra–Borneo region in December produces Kelvin wave-like low temperature anomalies in the tropical tropopause layer (TTL) over the eastern MC. These temperature anomalies strengthen when the lower stratospheric wind is easterly. We propose a hypothesis that the anomalous cooling associated with Kelvin wave-like response produces a favorable condition for a development of penetrating convection into the TTL over the eastern MC and more effective seasonal march of deep convection across the MC occurs under the QBO–E. The implication of this process for the QBO modulation of the MJO crossing the MC is also discussed.

Keywords QBO; MJO; penetrating convection; Stratosphere; Tropical tropopause

1. **Introduction**

A possible influence of the stratospheric quasi-biennial oscillation (QBO) on tropical convection has been reported since the mid-1980s (Gray, 1984; Collimore et al., 2003; Liess and Geller, 2012; see also the review by Haynes et al., 2021). The QBO influence on intra-seasonal oscillation (ISO) was also proposed by Kuma (1990) in 1990. However, only in recent studies (Yoo and Son, 2016; Son et al., 2017; Nishimoto and Yoden, 2017; Klotzbach et al., 2019), statistically significant impacts of the QBO on the ISO, known as a Madden–Julian Oscillation (MJO; Madden and Julian, 1972), were confirmed during the austral summer. A clear difference in the MJO between the QBO east (QBO–E) and west (QBO–W) is apparent when the active MJO convections move eastward across the Maritime Continent (MC) (Zhang and Zhang, 2018; Densmore et al., 2019; Barrett et al., 2021). However, the mechanism by which the MJO is influenced by the QBO remains unclear (see recent reviews by Jiang et al., 2020; Martin et al., 2021).

The vertical structure of the MJO is characterized by very deep convection reaching the tropical tropopause layer (TTL) or altitudes above 14 km (Morita et al., 2006; Kim et al., 2018). However, the MJO influence extends into the lower stratosphere by creating a Kelvin wave-like circulation response in the TTL (Eguchi and Shiotani, 2004; Virts and Wallace, 2010). Characteristic differences in the vertical structure of the MJO according to the phase of the QBO were demonstrated by Hendon and Abhik (2018). Their results reveal that low temperature anomalies tilt eastward with height from the western MC in the TTL to the lower stratosphere. Such anomalies get stronger during QBO-E austral summer, compared to QBO-W. They argued that the resultant stability decrease in the upper troposphere to the west of the convection center may help maintain convection behind the MJO, explaining a relatively slow propagation of the MJO during QBO–E.

Unlike previous studies that have focused on the seasonal-mean tropical convection and the time-filtered MJO convection, the present study examines the seasonal migration of tropical convection around the MC during the austral summer and its interannual change in response to the QBO.

Seasonal variation, in fact, is a response to the annual cycle in solar zenith angle. Such slow seasonal variation in solar radiative forcing may induces abrupt changes in monsoon activity through non-linear processes involved in the atmosphere-ocean system. According to this hypothesis, we also investigate sub-seasonal variation phase locked to the annual cycle. In fact, it is noted that the MJO tends to be phase-locked to the annual cycle during the early austral summer (Miura et al., 2015). In particular, onset of the Indonesian monsoon is related to the passage of the MJO around December (Duan et al., 2019). Such sub-seasonal variation phase locked to the annual cycle of the solar forcing should be similar to the "climatological ISO", defined by applying the ISO criteria to the climatological annual cycle

(Wang et al., 1997; Kikuchi et al., 2021), while this is not identical to the composite of the individual ISO events extracted by applying a space-temporal filter.

It should be stated that we mainly consider the seasonal migration of very deep convection that is derived from the calendar day mean. It differs from previous studies on the QBO-MJO connection in which MJO events are selected with spatiotemporal filtering.

In the present study we focus on low temperature anomalies to the east of the major convection center above the TTL, not the west below 100 hPa as in Hendon and Abhik (2018), and discuss their connection to the development of very deep convection penetrating into the TTL to the east, which manifests as eastward propagation of deep convection over the MC in austral summer.

2. **Data**

The meteorological fields are analyzed using meteorological reanalysis data from the Japan Meteorological Agency (JMA) JRA–55 (Kobayashi et al., 2015) on 1.25° latitude by 1.25° longitude grid cells during the satellite observation era since 1979. Interpolated outgoing longwave radiation (OLR) data with 2.5° × 2.5° grid cells (Liebmann and Smith, 1996) are provided by National Oceanic and Atmospheric Administration (NOAA). Cloud top pressure observed by the MODIS-TERRA satellite (Platnick et al., 2003), presented on 1° × 1° grid cells, is obtained from the GSFC/NASA GIOVANNI system. The climatology is defined as long-term mean over the period of 1979–2019, except for the MODIS-TERRA cloud data for the period 2000–2020. The standard deviation is calculated over the same period.

The phase of the QBO is defined by the direction of zonal-mean zonal winds at 70 hPa averaged over the equator. The equatorial region in the present study is taken as the latitudinal average from 5°S to 5°N. The El Niño/Southern Oscillation (ENSO) phenomenon is defined by the sea surface temperature (SST) averaged over the Niño 3 region (5°S–5N°, 150°W–90°W) using monthly mean gridded SST data from COBE (Ishii et al., 2005) with 1° × 1° grid cells.

3. **Results**

Seasonal march

Monsoonal convective activity progresses southeastward from the Indian Ocean to the Pacific following the seasonal march of the surface temperature and moisture distribution. This seasonal march around the MC is presented in Fig. 1a. Equivalent potential temperature increases over the eastern MC and the western Pacific from the end of November to December. Accordingly, convective activity migrates eastward, and the climatological onset of the austral summer monsoon over the MC around 120°E occurs in early December (Tanaka,1994; Duan2019).

Fig. 1

The eastward migration of convective activity occurs in a stepwise fashion following the location of large islands, as seen in Fig. 1. The convective activity expressed by the OLR is higher around large islands and moves southeastward with time (Fig. 2d). Eastward movement is particularly evident in very deep nighttime convection over land (Fig. 2c): i.e., Sumatra in November, Borneo and Java in December, and New Guinea in January.

Fig. 2

It is known that enhanced convective activity over the equator produces a Matsuno–Gill type circulation pattern (Matsuno, 1966; Gill, 1980) that is characterized by a combined equatorial Rossby and Kelvin wave-like circulation structure. The zonal gradient of temperature ($\partial T/\partial x$) over the equator, which is used as an index of Kelvin wave amplitude (Nishimoto and Shiotani, 2012), is indeed large over the eastern MC around the tropopause-lower stratosphere (Fig. 2a). Horizontal divergence in the TTL (Fig. 2b) is enhanced over the region of penetrating convection (Kodera et al., 2021). Thus, the anomalous low temperature tilted eastward with height over the equator suggests a Kelvin wave-like response produced by intense convection (Randel and Wu, 2005). Such anomaly is particularly evident in December (Fig. 2a). Thus, we focus on the December state in the following sections.

QBO impact in December

In order to examine the temperature and circulation changes in the TTL and lower stratosphere over the MC in response to the QBO, December mean states are first compared between the QBO–E and QBO–W. The sub-seasonal march is then considered in the next sub-section. The zonal-mean zonal wind at 70 hPa along the equator (5°N–5°S) is used to classify the 41 Decembers from 1979 to 2019 as either QBO–E or QBO–W. There are 21 easterly cases (1979, 1981, 1982, 1984, 1987, 1989, 1991, 1992, 1994, 1996, 1998, 2000, 2001, 2003, 2005, 2007, 2008, 2012, 2014, 2016, 2018), and 20 westerly cases (1980, 1983, 1985, 1986, 1988, 1990, 1993, 1995, 1997, 1999, 2002, 2004, 2006, 2009, 2010, 2011, 2013, 2015, 2017, 2019). Composites mean are then constructed for each QBO phase (Fig. 3).

Kelvin wave-like response as illustrated by $\partial T/\partial x$, is seen in Fig. 3a in the east of 100°E around the tropopause region for both QBO phases. In the case of the QBO–E, Kelvin wave-like response extends into the stratosphere over the eastern MC region in easterly winds, whereas, in the case of QBO–W, Kelvin wave-like response is very weak in the stratospheric westerlies. Such temperature signal is formed in association with upwelling in the upper troposphere over the western MC (100°–110°E), together with overhead downwelling (dotted lines in Fig. 3b) around the tropopause and lower stratosphere. In the case of the QBO–E, the anomalous downwelling at 70 hPa farther extends eastward. This is consistent with the fact that the equatorial Kelvin wave propagates vertically in the stratospheric easterlies and it becomes stronger and clear structure in the QBO-E state (Suzuki et al., 2010; Yang et al., 2012; Lim and Son, 2022).

Difference in standardized anomalous vertical velocity between the QBO–E and –W is largest in the eastern MC at 70 hPa. It is interesting to note that the difference is not significant over the western MC (100°–110°E) where deep convective clouds are frequently formed in December (see Fig. 2).

Equatorial deep convection penetrating into the TTL produces Kelvin wave-like response around the tropopause, of which vertical propagation in the stratosphere is affected by stratospheric zonal wind structure. Thus, connection between the QBO and penetrating convection can be represented by vertical velocity above the tropopause east of convection center in the troposphere. From the analysis in Fig. 3c, we consider the local monthly mean pressure vertical velocity (ω) at 70 hPa over 5°S–5°N and 140°–150°E (indicated by a box in Fig. 3c) as a response to tropospheric convection center around the western MC (100°–110°E). Therefore, this reference pressure vertical velocity (ω_{ref}) is utilized to study the downward influence of difference in Kelvin wave-like response around the tropopause region to the troposphere, as well as associated zonal wind in the stratosphere in Fig. 4.

Correlation coefficients between the ω_{ref} and zonal-mean zonal wind at each grid point in height-latitude cross-section exhibit a characteristic feature of the QBO with a seesaw in

Fig. 4

tropical zonal winds between middle and lower stratosphere (Fig.4a). Correlation between zonal winds over the equatorial region shows eastward tilted structure with height from the tropopause to the lower stratosphere over the eastern MC, adding to a zonal structure in the stratosphere (Fig.4b). Similarly, vertically tilted structure is also present in the temperature fields (Fig. 4c). Correlation map with the vertical velocity at each grid point (Fig. 4d) exhibits a pair of positive and negative dipole around the tropopause over the eastern MC. The latter negative correlation region extends downward from the TTL to the lower troposphere. Consistently, negative correlation is found with the OLR, in the eastern MC from Sulawesi to New Guinea (Fig. 4d). As a definition of the QBO phase, zonal mean zonal-winds at different stratospheric levels have been used by different authors. The correlation analysis in Fig. 4d using a local pressure vertical velocity over the eastern MC, shows positive and negative correlations with zonal mean zonal-winds over the equator at 10 and 70 hPa, respectively, which is a characteristic feature of the QBO zonal wind. This result gives a rationale for the use of 70 hPa zonal mean zona-wind to define the QBO in the present study.

The difference in OLR between the two QBO phases is more clearly illustrated in Fig. 5a. Fig. 5
The area where the difference is significant at the 90% and 95% confidence levels are indicated by shadings. Statistically significant differences are located mainly over the eastern MC. This result is not disturbed by the ENSO as shown in Fig. 5b where seven strong ENSO years exceeding ±1.5 standard deviation in Niño 3 December indices, i.e.,

three El Niño (1982, 1997, 2015) and four La Niña (1988, 1999, 2007, 2010) years, are excluded. The OLR difference over the eastern MC becomes even stronger without the strong ENSO years. It is noteworthy that the difference between the QBO phases concentrates in the equatorial belt (5°N-5°S; Fig. 5), while center of the convection resides in the south of the equator in December (Fig. 2d). This implies that the impacts of QBO on convection preferentially appear along the equatorial zone.

The results in this subsection suggest that interannual variability in vertical motion in the lower stratosphere over the eastern MC is well corelated with the deep convective activity through Kelvin wave-like circulation in the TTL. A possible causality between them will be discussed in the next subsection.

Sub-seasonal evolution

We investigate sub-seasonal evolution of the convection and the related fields around the MC to get insight into the causal relationship between the stratospheric variability and the convection. The sub-seasonal variation here is studied in terms of the deviation from the seasonal mean (75–day running mean) (Fig. 6). Calendar-day composite, instead of event composite such as the MJO, is constructed. The convective anomalies, whose evolutions are locked to the annual cycle, move from the eastern Indian Ocean to the western Pacific from late November to early January (Fig. 1a).

Fig. 6

The convective activities defined as anomalous OLR from the climatology, are similar for QBO–E and –W cases in late November (Fig. 6, top panels). In early December, horizontal divergence in the TTL strengthens around 120°E over the eastern MC for the QBO–E. This increased horizontal divergence in the stratosphere at 70hPa in early December precedes a decreased OLR in late December over the eastern MC. This suggests that eastern part of the Kelvin wave-like response, the tilted cold anomalies around the tropopause, may work to produce a vanguard convective activity before the arrival of the main body of the convection. However, it is still difficult to demonstrate detailed processes involving very small and deep convective activity. This could be because the change in the mesoscale convective system is obscured by the averaging process in the analysis.

To elucidate the relationship between the Kelvin wave-like response in the TTL and penetrating convection into the TTL, a case study is further conducted for the QBO–E case in December 2018. Figure 1c indicates that ISO signal in December 2018 is phase-locked to the onset of monsoon over the eastern MC. This ISO signal is also identified as a typical MJO event, as it is illustrated in a review paper (Jian et al., 2020). The seasonal evolutions of OLR and equivalent potential temperature at 850 hPa of this year are extracted in Fig. 1b by applying a 75-day running mean. Their seasonal evolutions in 2018-19 are very similar to the climatological seasonal evolutions shown in Fig. 1a.

The evolution of convective activity in December 2018 is displayed in Fig. 7. Anomalous temperature from climatology and pressure vertical velocity are displayed in Fig. 7a, while Fig. 7b presents horizontal distribution of the OLR. Because the diurnal cycle is very pronounced over land, MODIS-TERRA cloud top pressure (CTP) during the night and day are presented separately in Figs. 7c and 7d, respectively.

Fig. 7

Convective activity develops over the Indian Ocean from 8 December. Enhanced upwelling over the convective center produces cooling around the tropopause over the Indian Ocean. The upward propagating Kelvin wave-like response produces a pair of temperature anomalies in the stratosphere on 11 December: a warm anomaly overlying a cool anomaly. The development of low temperature anomalies in the TTL over Sumatra coincides with a strong convective activity during the nighttime over land. A Rossby wave-like structure in the troposphere with vortices (not shown) both sides of the equator develops in association with daytime convective activity over the Indian Ocean. Kelvin wave-like structure in the stratosphere further develops on 14 December, and the anomalous cooling region in the TTL extends eastward over the eastern MC. At the same time, convection over Borneo and New Guinea Islands intensify during the night. While no clear activity in daytime convection is found over the eastern MC sector, daytime convective systems over the Indian Ocean, associated with the vortices each side of the equator, move to the off-equatorial direction.

The Kelvin wave-like structure around the tropopause propagates further eastward on 17 December, and convection over the eastern MC becomes active during both night and day. On the other hand, anomalous warming associated with the Kelvin wave-like response arrives over the Indian Ocean around 90°E, before a suppression of convective activity arrives there.

The above result suggests that the nighttime penetrating convection into TTL around 14 December plays an important role in eastward propagation of convection by generating a vanguard convective activity over the eastern MC through interaction with low temperature anomalies associated with the Kelvin-wave like response in the lower stratosphere. To elucidate this process, convective activity over the IO and the central MC are further compared by using daily mean data. Height-time cross-section of anomalous pressure vertical velocity is displayed by contours in Figs. 8 a–c, together with (a) temperature, (b) horizontal divergence, and (c) specific humidity anomalies, illustrated by color shadings. The OLR anomaly is also displayed in Fig. 8d to indicate usual convective activity.

Fig. 8

Over the IO (90°–100°E), increase in water vapor in the lower troposphere precedes the enhanced convective activity on 8 December (Fig. 8c). Increased upwelling, suggested by enhanced horizontal divergence, is accompanied with a large cooling at the tropopause from 10 December. While enhanced convective activity continues in the troposphere, warm temperature anomaly develops in the lower stratosphere on 14 December. This warm anomaly is related with a vertical propagation of the Kelvin wave-like signal shown in Fig. 7. As the Kelvin wave-like signal propagates eastward and water vapor in the lower troposphere decreases, the convective activity over the IO becomes weakened on 15 December.

Over the MC sector (115°–125°E), cold anomaly develops from 11 December in the lower stratosphere at 70 hPa in association with enhanced Kelvin wave-like response to convective activity over the IO in the west (Fig. 7a; Fig. 8a). A pair of positive and negative horizontal divergence at 70 and 150 hPa suggests a development of upward motion across the tropopause on 13 December (Fig. 8b). Anomalous upwelling then extends downward to the bottom of the TTL on 14 December, which coincides with a development of very deep nighttime convection over the eastern MC illustrated in Fig. 7. From 15 December, upwelling also increases in the lower troposphere as deep convective activity develops (Fig. 8d). Then, a cold temperature anomaly at 70 hPa is replaced by a warm anomaly on 17 December (Fig. 8a), consistent with eastward propagation of Kelvin wave-like temperature anomalies in Fig. 7a. In the case of the MC, no clear increase in water vapor is found in the lower troposphere prior to the development of the convection over the equatorial zone, nor in the equatorial SH. Water vapor in the middle troposphere rather increases following the convective activity from 17 to 20 December. These results suggest that the eastward migration of convection over the MC during the QBO–E in December 2018 was promoted by the Kelvin wave-like response in the TTL, rather than lower tropospheric water vapor accumulation.

4. **Summary and discussion**

The present study examines seasonal and sub-seasonal migration of tropical convection in response to the QBO phase locked to the annual cycle during the austral summer around the MC. The results are summarized as follows. Convective activity over the MC region intensifies during the austral summer monsoon in December. The associated Kelvin wave-like response appears in the TTL over the eastern MC (Fig. 2). Connection between the QBO stratospheric zonal wind and the deep convection over the MC is hypothesized to be produced through Kelvin-wave response around the tropopause region (Fig. 3). Vertical velocity, modulated by the QBO zonal wind, is likely connected to the OLR over the eastern MC (Fig. 4). Their relationship becomes clearer when ENSO-related years are eliminated (Fig. 5).

The analysis of intra-seasonal evolutions of the convection and the related fields over the MC, which are phase-locked to the annual cycle, suggests that a generation of vanguard convection penetrating into the TTL during the night in the eastern MC occurs in connection with a downward extension of horizontal divergence from early to late December during the QBO-E (Fig. 6). The role of penetrating convection into the TTL in eastward propagation of convective center over the MC region is further studied by taking the 2018 December QBO–E case. The eastward shift of convective center over the eastern MC is initiated by the development of penetrating convection into the TTL over land during the nighttime (14 December in Fig. 7). The increased water vapor in the lower troposphere precedes the convection over the IO (Fig. 8), consistent with an eastward propagation of upwelling from the lower troposphere. Contrastingly, development of upwelling is initiated from the tropopause level and deep convection over the MC is amplified in the troposphere with little increase in water vapor in the lower troposphere prior to the convective activity. This case study supports the idea that the TTL process can play an important role in the eastward propagation of convection over the MC. This result is also consistent with the analysis of Barret et al. (2021) that MJO events during QBO–W need more water vapor to cross the MC than during QBO–E.

According to these results, we propose a following working hypothesis as schematically represented in Fig. 9: Convective activity over the Sumatra–Borneo sector (light blue area with dashed contour) induces Kelvin wave-like low temperature anomalies around the tropopause region (light blue area with closed contour), which are stronger under QBO–E (left panel). Enhanced cold anomalies in the TTL promote a development of penetrative deep convection as vanguard convective activity around New Guinea over the eastern MC during QBO–E. It strengthens an eastward migration of convective activity across the MC

Fig. 9

by further producing usual convective activity over the western Pacific. In other words, convective activity over the Sumatra–Borneo region can migrate more easily eastward during QBO–E by instigating vanguard deep convective activity over the eastern MC sector. In the case of QBO–W (right panels), the Kelvin wave-like response is suppressed in the stratosphere, making a smaller impact in the TTL. Accordingly, its impact on convective activity in the eastern MC is smaller, and eastward propagation of convection becomes unclear.

It is noteworthy that Peatman et al. (2014) argued that relatively clear skies east of the major convective center of the MJO can create enhanced heating over land to destabilize the atmosphere. However, they did not show the process through which the convective center migrates over the MC from the western to the eastern MC. Birch et al. (2015) emphasized the importance of the scale interactions among the local deep convection over land and the large-scale moisture accumulation over the ocean to the MJO progression over the western MC. However, their focuses were rather on the lower tropospheric and surface processes. We suggest in the present study that the cooling in the TTL due to the Kelvin wave-like temperature response is important to enhance vanguard penetrative convection in the eastern MC, especially along the equatorial zone. Although the southward path over the surrounding ocean over the land area of the MC is a subtle feature of the MJO cases that successfully crossing over the MC (Zhang and Ling 2017), our finding suggests that the

QBO phases possibly affect the MJO propagation (specifically from central to eastern MC) via Kelvin-wave deep-convection interactions in the equatorial zone.

In terms of the analogy with the MJO, convective activity over land is believed to work as a barrier to the propagation of the MJO across the MC (Zhang and Ling, 2017; Ling et al., 2019). Yuan and Houze, (2013) demonstrated that a discrete mesoscale convection system shows clear eastward propagation over the islands of the MC, while large mesoscale convection system over the sea remains stationary. This is consistent with the present analysis in Fig. 7, where penetrating convection into the TTL over land propagates eastward in connection with low temperature anomalies in the TTL. Furthermore, nighttime land convective activity can also induce convection on the following day over the ocean (Ichikawa and Yasunari, 2007; Sakaeda et al, 2020).

In this study, we suggest that low temperature anomalies associated with the Kelvin wave to the east of the major convective center (Lim and Son, 2022) could also play an important role by interacting with penetrating deep convection in the TTL. Hendon and Abhik (2018) suggested that TTL cold anomalies extending downward and westward may allow development of deep convection to the west of previous convection, causing a rather slow MJO propagation during QBO-E. However, such downward extension does not appear over the western MC.

Concerning the convective activity associated with the MJO, penetrating convection into the TTL develops east of the main convective center (see Fig. 6a of Morita et al., 2006; Fig. S2 of Kim et al., 2018). This is consistent with a separate upwelling region in the TTL about 30° east of the main convective center of the MJO (Fig. S1 Phase 4 of Hendon and Abhik 2018). Such upwelling in TTL in the east is related with tropospheric convective activity during QBO–E, but little connected to the troposphere during QBO–W, similar to the difference in our results in Fig. 3.

Relatively clear skies ahead of the main convective center of the MJO may produce unstable tropospheric condition by increased surface heating over lands. The major question is whether the very deep mesoscale convection penetrating into the TTL can be robustly induced under such tropospheric condition by anomalous stratospheric cooling associated with the Kelvin wave-like response.

To elucidate such a causal relationship between the deep convection and a stratospheric cooling at intraseasonal time scale, model study is crucial. However, the effect of mesoscale convection penetrating into the TTL is difficult to simulate with conventional general circulation models (GCMs). Therefore, it is not surprising to find that the QBO modulation of the MJO is missing in GCM simulations (Kim et al., 2020; Lim and Son, 2020). Indeed, a numerical model experiment of Martin et al. (2021) by nudging the model stratosphere to the observation can reproduce a Kelvin wave-like response in the TTL, but failed to reproduce the QBO effect in the troposphere. On the other hand, the experiment of Back et al. (2020) using a regional model in a horizontal resolution of 9 km, capable of resolving mesoscale convection systems, can reproduces the QBO impact, although the amplitude is still much smaller. We hope advanced cloud resolving global models could clarify the role of the mesoscale convection system in future studies on connection between the stratosphere and troposphere.

Data Availability Statement

All datasets analyzed in this study are publicly available: JRA-55 reanalysis data at [https://jra.kishou.go.jp/JRA-55/index_en.html#jra-55], COBE SST data at [https://ds.data.jma.go.jp/tcc/tcc/products/elnino/cobesst/cobe-sst.html], NOAA OLR at [https://psl.noaa.gov/data/gridded/data.interp_OLR.html], MODIS data through GIOVANNI system at [https://giovanni.gsfc.nasa.gov/giovanni/].

Acknowledgments

Preliminary analysis of this study was carried out using the Interactive Tool for Analysis of the Climate System (ITACS) provided by the Japan Meteorological Agency. OLR data are provided by NOAA (https://psl.noaa.gov/data/gridded/data.interp_OLR.html). Analyses of

MODIS data in this study were produced with the Giovanni online data system, developed and maintained by the NASA GES DISC. This work was supported in part by Grants-in-Aid for Scientific Research (25340010, 17H01159, JP18K03743, JP21H01156) from the Japan Society for the Promotion of Science. SWS was supported by the National Research Foundation of Korea (NRF) grant funded by the Korea government (MSIT) (2023R1A2C3005607).

References

Back, S.-Y., J.-Y. Han, and S.-W. Son, 2020: Modeling evidence of QBO–MJO connection: A case study. *Geophys. Res. Lett.*, **47**, e2020GL089480, doi:10.1029/2020GL089480.

Barrett, B.S., C.R. Densmore, P. Ray, and E.R. Sanabia1, 2021: Active and weakening MJO events in the Maritime Continent. *Clim Dyn*. **57**, 157–172. https://doi.org/10.1007/s00382-021-05699-8

Birch, C., S. Webster, S. C. Peatman, D. Parker, A. Matthews, Y. Li, and M. Hassim, 2016: Scale interactions between the MJO and the western Maritime Continent. *J. Climate*, 29, 2471−2492, doi:10.1175/JCLI-D-15-0557.1.

Collimore, C. C., D. W. Martin, M. H. Hitchman, A. Huesmann, and D. E. Waliser, 2003: On the relationship between the QBO and tropical deep convection. *J. Climate*, **16**, 2552–2568.

Densmore, C.R., E.R. Sanabia, and B.S. Barrett, 2019: QBO influence on MJO amplitude over the Maritime Continent: Physical mechanisms and seasonality. *Mon. Wea. Rev.*, **147**, 389– 406, https://doi.org/10.1175/MWR-D-18-0158.1

Duan, Y., H. Liu, W. Yu, L. Liu, G. Yang, and B. Liu, 2019: The onset of the Indonesian–Australian summer monsoon triggered by the first-branch eastward-propagating Madden–Julian oscillation. *J. Climate*, **32**, 5453–5470, https://doi.org/10.1175/JCLI-D-18-0513.1.

Eguchi, N., and M. Shiotani, 2004: Intraseasonal variations of water vapor and cirrus clouds in the tropical upper troposphere. *J. Geophys. Res.*, **109**, D12106, doi:10.1029/2003JD004314.

Gill, A. E.,1980: Some simple solutions for heat-induced tropical circulation. *Q. J. R. Meteorol. Soc.*, **106**, 447– 462.

Gray, W.M., 1984: Atlantic seasonal hurricane frequency. Part I: El Niño and 30 mb quasi-biennial oscillation influences. *Mon. Wea. Rev.*, **112**, 1649–1668.

Haynes, P. H., P. Hitchcock, M. H. Hitchman, S. Yoden, H. Hendon, G. Kiladis, K. Kodera, and I. Simpson, 2021: Stratosphere-troposphere coupling in the tropics. *J. Meteorol. Soc. Jpn.*, https://doi.org/10.2151/jmsj.2021-040

Hendon, H. H., and S. Abhik, 2018: Differences in vertical structure of the Madden–Julian Oscillation associated with the quasi-biennial oscillation. *Geophys. Res. Lett.*, **45**, 4419–4428. https://doi.org/10.1029/2018GL077207

Ichikawa, H., and T. Yasunari, 2007: Propagating diurnal disturbances embedded in the Madden–Julian Oscillation, *Geophys. Res. Lett.*, **34**, L18811, doi:10.1029/2007GL030480

Ishii, M., A. Shouji, S. Sugimoto, and T. Matsumoto, 2005: Objective analyses of sea-surface temperature and marine meteorological variables for the 20th century using ICOADS and the KOBE collection. *Int. J. Climatol.*, **25**, 865–879.

Jiang, X., Adames, Á. F., Kim, D., Maloney, E. D., Lin, H., Kim, H., et al., 2020: Fifty years of research on the Madden-Julian Oscillation: Recent progress, challenges, and perspectives. *J. Geophys. Res. Atmos.*, **125**, e2019JD030911. https://doi.org/10.1029/2019JD030911

Kikuchi, K., B. Wang, and Y. Kajikawa, 2012: Bimodal representation of the tropical intraseasonal oscillation. *Climate Dyn.*, **38**, 1989–2000, doi:10.1007/s00382-011-1159-1.

Kim, H., Caron, J. M., Richter, J. H., and Simpson, I. R., 2020: The lack of QBO–MJO connection in CMIP6 models. *Geophys. Res. Lett.*, **47**, e2020GL087295. https://doi.org/10.1029/2020GL087295

Kim, J., Randel, W. J., & Birner, T., 2018: Convectively driven tropopause-level cooling and its influences on stratospheric moisture. *J. Geophys. Res.*, **123**. https://doi.org/10.1002/2017JD027080

Klotzbach, P., S. Abhik, H. Hendon, M. Bell, C. Lucas, A. Marshall, and E. Oliver, 2019: On the emerging relationship between the stratospheric quasi-biennial oscillation and the Madden-Julian oscillation. *Scientific Reports*, **9**(1), 2981

Kobayashi, S., Y. Ota, Y. Harada, A. Ebita, M. Moriya, H. Onoda, K. Onogi, H. Kamahori, C. Kobayashi, H. Endo, K. Miyaoka, and K. Takahashi, 2015: The JRA–55 reanalysis:

General specifications and basic characteristics. *J. Meteor. Soc. Japan*, **93**, 5−48.

Kodera, k., N. Eguchi, R. Ueyama, B.M. Funatsu, M. Gaetani, and C.M. Taylor, 2021: The Impact of tropical tropopause cooling on Sahelian extreme deep convection. *J. Meteor. Soc. Jap.*, https://doi.org/10.2151/jmsj.2021-055

Kuma, K, 1990: A quasi-biennial oscillation in the intensity of the intraseasonal oscillation. *Int. J. Climatol*., **10**, 263-278.

Liess, S., and M. A. Geller, 2012: On the relationship between QBO and distribution of tropical deep convection. *J. Geophys. Res.*, **117**, D03108, doi:10.1029/2011JD016317.

Liebmann, B., and C. A. Smith, 1996: Description of a complete (interpolated) outgoing longwave radiation dataset. *Bull. Amer.Meteor. Soc.*, **77**, 1275–1277.

Lim, Y., and S.-W. Son, 2020: QBO-MJO connection in CMIP5 Models. *J. Geophys. Res. Atmos.*, **125**, e2019JD032157.

Lim, Y., and S.-W. Son, 2022: QBO Wind Influence on MJO-Induced temperature anomalies in the upper troposphere and lower stratosphere in an idealized model. *J. Atmos. Sci.*, **79**, 2219–2228, https://doi.org/10.1175/JAS-D-21-0296.1.

Ling, J., Zhao, Y., and G. Chen, 2019: Barrier effect on MJO propagation by the Maritime Continent in the MJO Task Force/GEWEX Atmospheric System Study Models. *J. Clim.*, **32**, 5529–5547.

Madden, R. A., and P.R. Julian, 1972: Description of global-scale circulation cells in the tropics with a 40–50 day period. *J. Atmos. Sci.*, **29**, 1109–1123.

Martin, Z., C. Orbe, S. Wang, and A. Sobel, 2021: The MJO–QBO Relationship in a GCM with Stratospheric Nudging. *J. Climate*, **34**, 4603–4624, https://doi.org/10.1175/JCLI-D-20-0636.1

Matsuno, T.,1966: Quasi-geostrophic motions in the equatorial area. *J. Meteor. Soc. Jpn.*, **44**, 25– 43.

Miura, H., T. Suematsu, and T. Nasuno, 2015: An ensemble hindcast of the Madden-Julian Oscillation during the CINDY2011/DYNAMO field campaign and influence of seasonal variation of sea surface temperature. *J. Meteor. Soc. Jpn*, **93A**, 115-137, 797 doi:10.2151/jmsj.2015-055.

Morita, J., Y. N. Takayabu, S. Shige, and Y. Kodama, 2006: Analysis of rainfall characteristics of the Madden–Julian oscillation using TRMM satellite data. *Dyn. Atmos. Oceans*, **42**, 107– 126, https:// doi.org/10.1016/j.dynatmoce.2006.02.002.

Nishimoto, E., and M. Shiotani, 2012: Seasonal and interannual variability in the temperature structure around the tropical tropopause and its relationship with convective activities. *J. Geophys. Res.*, **117**, D02104, doi:10.1029/2011JD016936.

Nishimoto, E., and S. Yoden, 2017: Influence of the stratospheric quasi-biennial oscillation on the Madden–Julian oscillation during austral summer. *J. Atmos. Sci.*, **74**, 1105–1125, https://doi.org/10.1175/JAS-D-16-0205.1.

Peatman, S. C., A. J. Matthews, and D. P. Stevens, 2014: Propagation of the Madden–Julian oscillation through the Maritime Continent and scale interaction with the diurnal cycle of precipitation. *Quart. J. Roy. Meteorol. Soc.*, **140**, 814–825, doi:10.1002/qj.2161.

Platnick, S., M. D. King, S. A. Ackerman, W.P. Menzel, B.A. Baum, J.C. Jérôme, R.A. Frey, 2003: The MODIS cloud products: Algorithms and examples from Terra. *IEEE Trans. Geosci. Remote Sens.*, **41**, 459–473. DOI:10.1109/TGRS.2002.808301

Randel, W. J., and F. Wu, 2005: Kelvin wave variability near the equatorial tropopause observed in GPS radio occultation measurements. *J. Geophys. Res.*, **110**, D03102, doi:10.1029/2004JD005006.

Sakaeda, N., Dias, J., and Kiladis, G. N., 2020: The unique characteristics and potential mechanisms of the MJO–QBO relationship. *J. Geophys. Res.: Atmospheres*, **125**, e2020JD033196. https://doi.org/10.1029/2020JD033196

Son, S.-W., Y. Lim, C. Yoo, H. H. Hendon, and J. Kim, 2017: Stratospheric control of Madden–Julian oscillation. *J. Clim.*, **30**, 1909–1922, doi:10.1175/JCLI-D-16-0620.1.

Suzuki, J., M. Shiotani, and N. Nishi, 2010: Lifetime and longitudinal variability of equatorial Kelvin waves around the tropical tropopause region, *J. Geophys. Res.*, **115**, D03103, doi:10.1029/2009JD012261.

Tanaka, M., 1994: The onset and retreat dates of the austral summer monsoon over Indonesia, Australia and New Guinea. *J. Meteor. Soc. Jpn*, **72**, 255–267, https://doi.org/10.2151/jmsj1965.72.2_255.

Virts, K. S., and Wallace, J. M., 2014: Observations of temperature, wind, cirrus, and trace gases in the tropical tropopause transition layer during the MJO. *J. Atmos. Sci.*, **71**, 1143–

1157.

Wang, B., and X. Xu, 1997: Northern Hemisphere summer monsoon singularities and climatological intraseasonal oscillation. *J. Clim.*, **10**, 1071–1085.

Yang, G.-Y., B., Hoskins, and L. Gray, 2012: The influence of the QBO on the propagation of equatorial waves into the stratosphere. *J. the Atmos. Sci.*, **69**, 2959–2982. https://doi.org/10.1175/JAS-D-11-0342.1

Yoo, C., and S.-W. Son, 2016: Modulation of the Austral summertime Madden–Julian oscillation by the stratospheric quasi-biennial oscillation. *Geophys. Res. Lett.*, **43**, doi:10.1002/ 2016GL067762.

Yuan, J., and R. A. Houze, 2013: Deep convective systems observed by A-Train in the tropical Indo-Pacific region affected by the MJO. *J. Atmos. Sci.*, **70**, 456–486, doi:10.1175/JAS-D-12-057.1

Zhang, C., and J. Ling, 2017: Barrier effect of the Indo–Pacific Maritime Continent on the MJO: Perspectives from tracking MJO precipitation. *J. Clim.*, **30**, 3439–3459, https://doi.org/10.1175/JCLI-D-16-0614.1

Zhang, C., and B. Zhang, 2018: QBO-MJO connection. *J. Geophys. Res. Atmos.*, **123**, 2957– 2967, https://doi.org/10.1002/2017JD028171

List of Figures

Fig. 1 (a) Time–longitude cross-section of daily climatology over the equator (5°S–5°N) with equivalent potential temperature at 850 hPa (color shading) and OLR (contours: 190, 200, 210 Wm^{-2}). (b) Similar to (a), but for 75-day running mean daily data for the year 2018/19. (c) Similar to (b), but for 7-day running mean data. (contours: 160, 180, 200 Wm^{-2}) (d) Land distribution.

Fig. 2 Monthly mean climatology for November (left), December (middle), and January (right). (a) Height–longitude cross-sections of climatological eastward air temperature gradient ($\partial T/\partial x$) (color shading) and horizontal divergence (contours: −3.6, −3.0, −2.4, -1.8×10^{-6} s^{-1}). (b) Horizontal divergence at 125 hPa. (c) Cloud top pressure (CTP) distribution observed by MODIS TERRA night pass. (d) OLR.

Fig. 3 (a and b) Composite means for QBO–E (left) and QBO–W (right) in December over the equator (5°S–5°N). (a) Zonal winds (color shading) and eastward temperature gradient < 0 (contours: every 2×10^{-7} K m^{-1}). (b) Pressure vertical velocity <0 (contours: every 0.02 Pa s^{-1}) and its normalized anomaly at each grid (color shadings). (c) Same as (b), except for difference between QBO–E and QBO–W. Box in (c) indicates the area used for define the reference index ω_{ref} in Fig. 4.

Fig. 4 Correlation coefficients between ω_{ref} (ω at 70 hPa, 140°–150°E, 5°S–5°N; indicated by thick black line in (d)), and anomalous (a) zonal-mean zonal winds for December 1979–2019. (b–d) Same correlation coefficient between ω_{ref} except for equatorial (5°S–5°N) (b) zonal wind, (c) temperature, and (d) pressure vertical velocity. (e) Same as (a) except for correlation between OLR. Contour interval is 0.1 from −0.55 to 0.55 and statistical significance higher than 95% level is shown by color shadings.

Fig. 5 (a) Composite mean differences of OLRs between QBO–E and W in December (1979–2019). Contours are every 3 Wm^{-2} with 0 lines suppressed. Positive and negative values are indicated by cold and warm color, respectively. Statistical significance higher than 90 and 95% levels are indicated by shadings (b) Same as (a), but for seven ENSO-related years have been eliminated.

Fig. 6 Composite means of intra-seasonal variation locked to the annual cycle for QBO–E, (a and b) and QBO–W (c and d). Figs. (a and c) show anomalous temperature (color shadings) and horizontal divergence >0 (contours: 0.5, 1, 1.5 $\times 10^{-6}$ s^{-1}), respectively. Figs. b and d shows anomalous OLR. From the top to bottom, 15-day means over 16–30 November, 1–15 December, 16–30 December, and 21 December–14 January.

Fig. 7 Intraseasonal component during 2018. (a) Longitude–height cross-sections over the equator (5°S-5°N) for anomalous temperature from climatology (color shading) and pressure vertical velocity < 0 (contours: every −0.05 hPa s^{-1}). (b) OLR. (c) Cloud top pressure from satellite nighttime passes. (d) Same as (c), but from daytime passes. (From top bottom) Consecutive 3-day mean data centered on 8, 11, 14, and 17 December 2018. Letters IO, S, B, N indicate longitudinal position of the Indian Ocean, Sumatra, Borneo, and New Guinea.

Fig. 8 Time evolution of daily mean data at two locations over the equator (5°S-5°N) over (left) IO (90°-100°E, 5°S-5°N) and (right) MC (115°-125°E, 5°S-5°N). (a-c) Height-time cross-sections of anomalous variables: (a) temperature, (b) horizontal divergence and (c) specific humidity are shown by color shadings, while pressure vertical velocity is shown by contours in a, b, c for $\omega<0$ (-0.1,-0.075, -0.05, -0.025, -0.01, -0.005 hPa s^{-1}). (d) anomalous OLR. Vertical lines indicate the dates 11, and 16 December 2018.

Fig. 9 Schematics of “Kelvin wave bridge” over the Maritime Continent. Letters S, B, N denote Sumatra, Borneo, and New Guinea islands. Wa and Co denote warm and cool anomalies. Arrows indicate vertical and horizontal winds. Cyclonic circulation is noted by c. (See text for more detail).

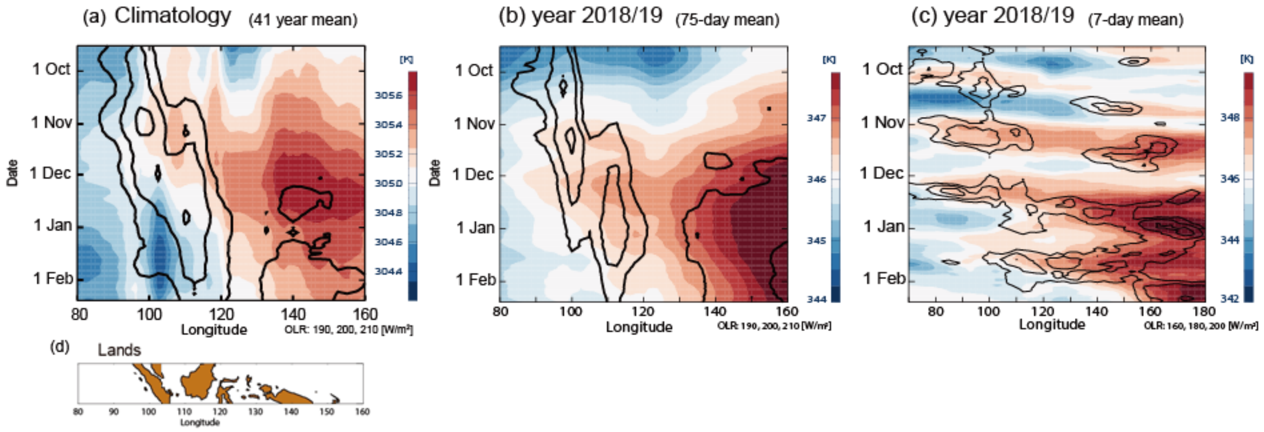

Fig. 1 (a) Time–longitude cross-section of daily climatology over the equator (5°S–5°N) with equivalent potential temperature at 850 hPa (color shading) and OLR (contours: 190, 200, 210 Wm^{-2}). (b) Similar to (a), but for 75-day running mean daily data for the year 2018/19. (c) Similar to (b), but for 7-day running mean data. (contours: 160, 180, 200 Wm^{-2}) (d) Land distribution.

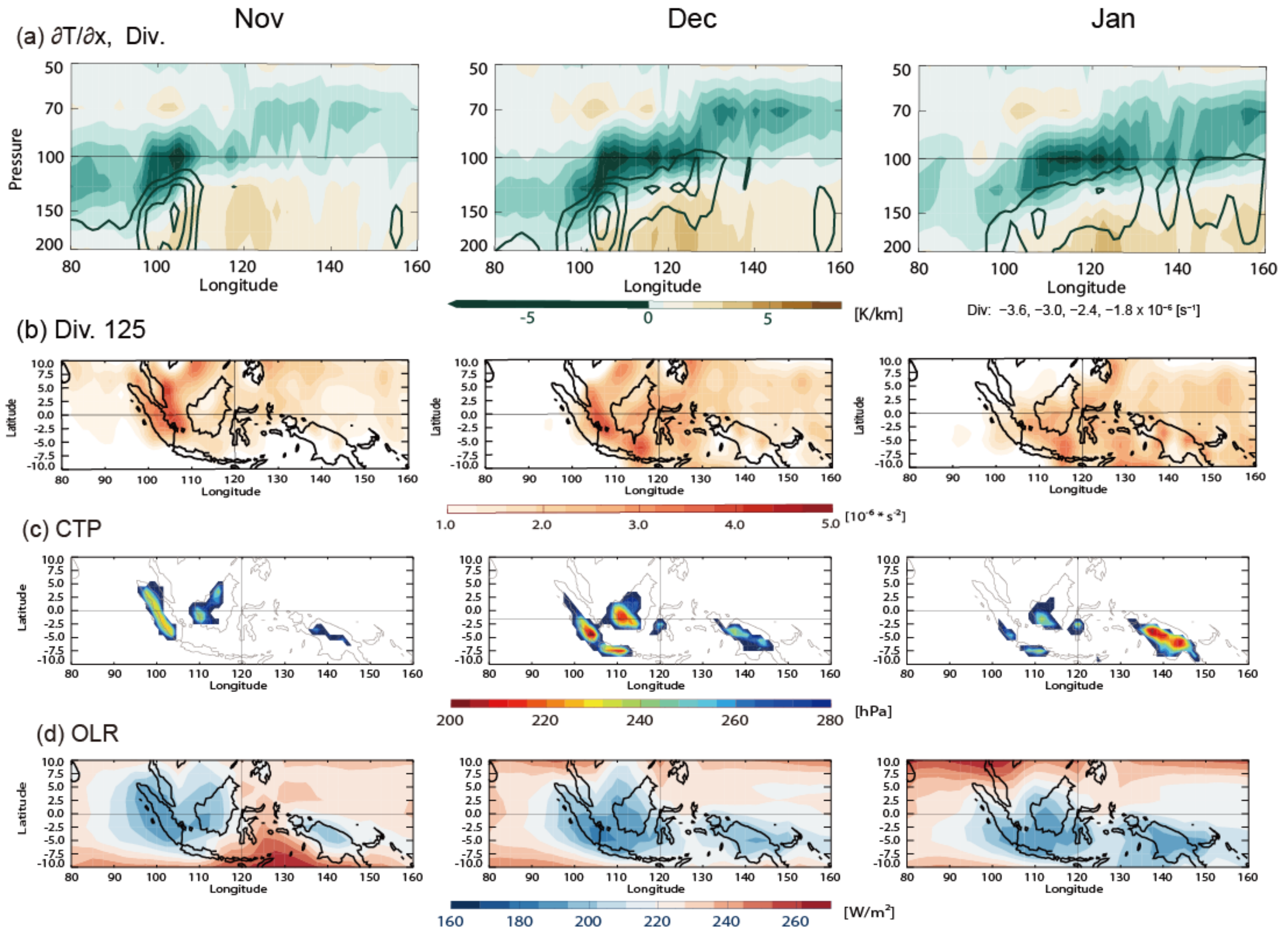

Fig. 2 Monthly mean climatology for November (left), December (middle), and January (right). (a) Height–longitude cross-sections of climatological eastward air temperature gradient ($\partial T/\partial x$) (color shading) and horizontal divergence (contours: −3.6, −3.0, −2.4, −1.8 $\times$ 10^{-6} s^{-1}). (b) Horizontal divergence at 125 hPa. (c) Cloud top pressure (CTP) distribution observed by MODIS TERRA night pass. (d) OLR.

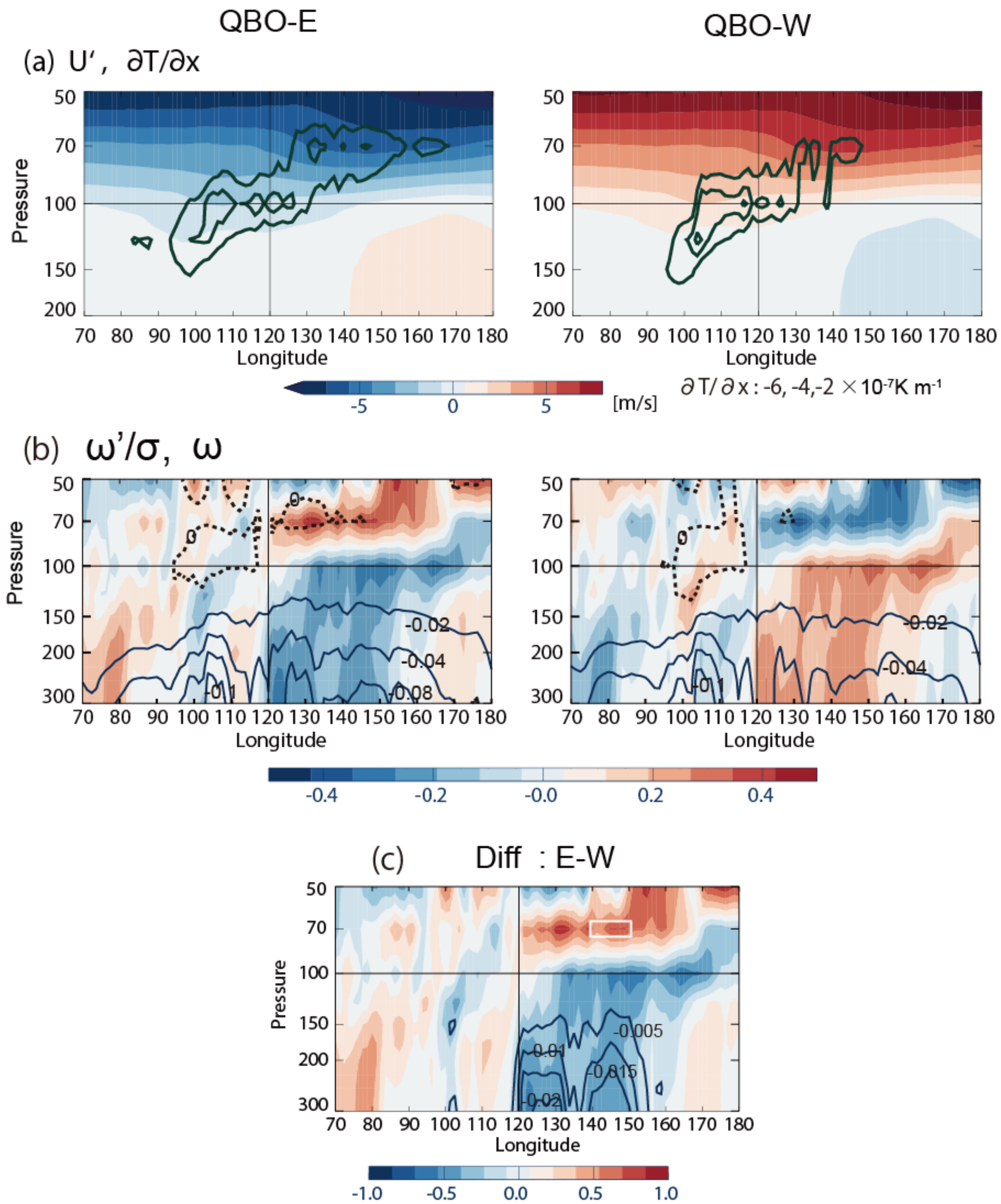

Fig. 3 (a and b) Composite means for QBO–E (left) and QBO–W (right) in December over the equator (5°S–5°N). (a) Zonal winds (color shading) and eastward temperature gradient < 0 (contours: every 2×10^{-7} K m^{-1}). (b) Pressure vertical velocity <0 (contours: every 0.02 Pa s^{-1}) and its normalized anomaly at each grid (color shadings). (c) Same as (b), except for difference between QBO–E and QBO–W. Box in (c) indicates the area used for define the reference index ω_{ref} in Fig. 4.

651

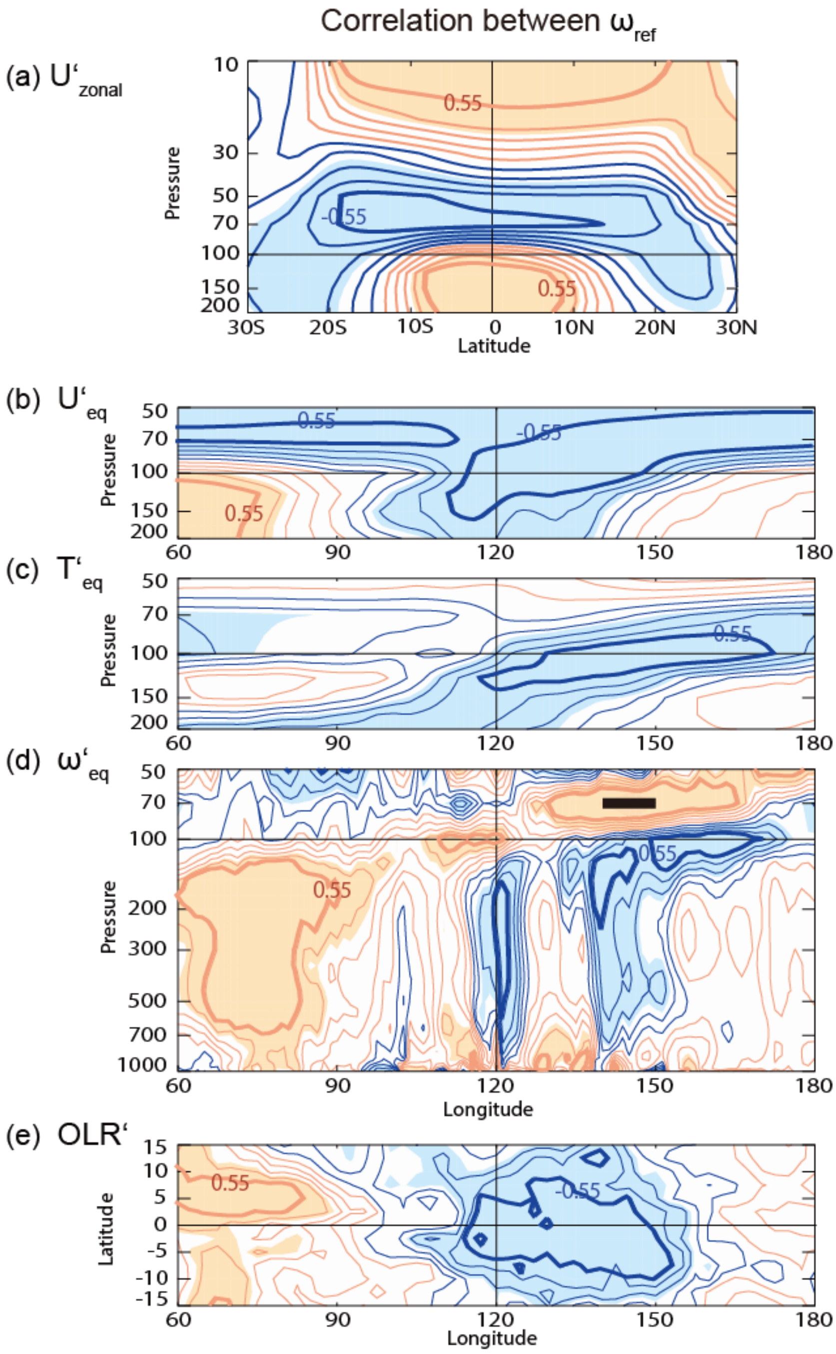

652 Fig. 4 Correlation coefficients between ω_{ref} (ω at 70 hPa, 140°–150°E, 5°S–5°N; indicated
653 by thick black line in (d)), and anomalous (a) zonal-mean zonal winds for December
654 1979–2019. (b–d) Same correlation coefficient between ω_{ref} except for equatorial (5°S–
655 5°N) (b) zonal wind, (c) temperature, and (d) pressure vertical velocity. (e) Same as (a)
656 except for correlation between OLR. Contour interval is 0.1 from −0.55 to 0.55 and
657 statistical significance higher than 95% level is shown by color shadings.

658

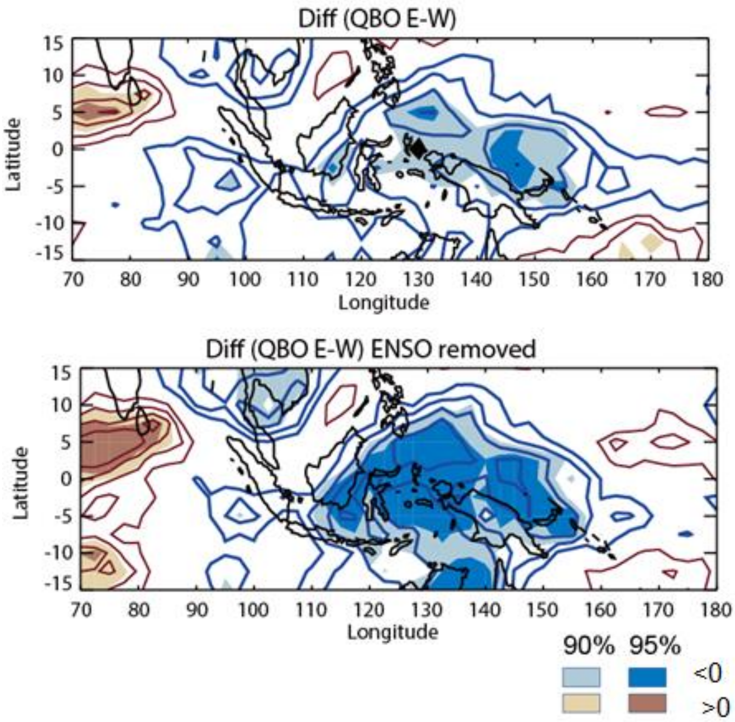

Fig. 5 (a) Composite mean differences of OLRs between QBO–E and W in December (1979–2019). Contours are every 3 Wm^{-2} with 0 lines suppressed. Positive and negative values are indicated by cold and warm color, respectively. Statistical significance higher than 90 and 95% levels are indicated by shadings. (b) Same as (a), but for seven ENSO-related years have been eliminated.

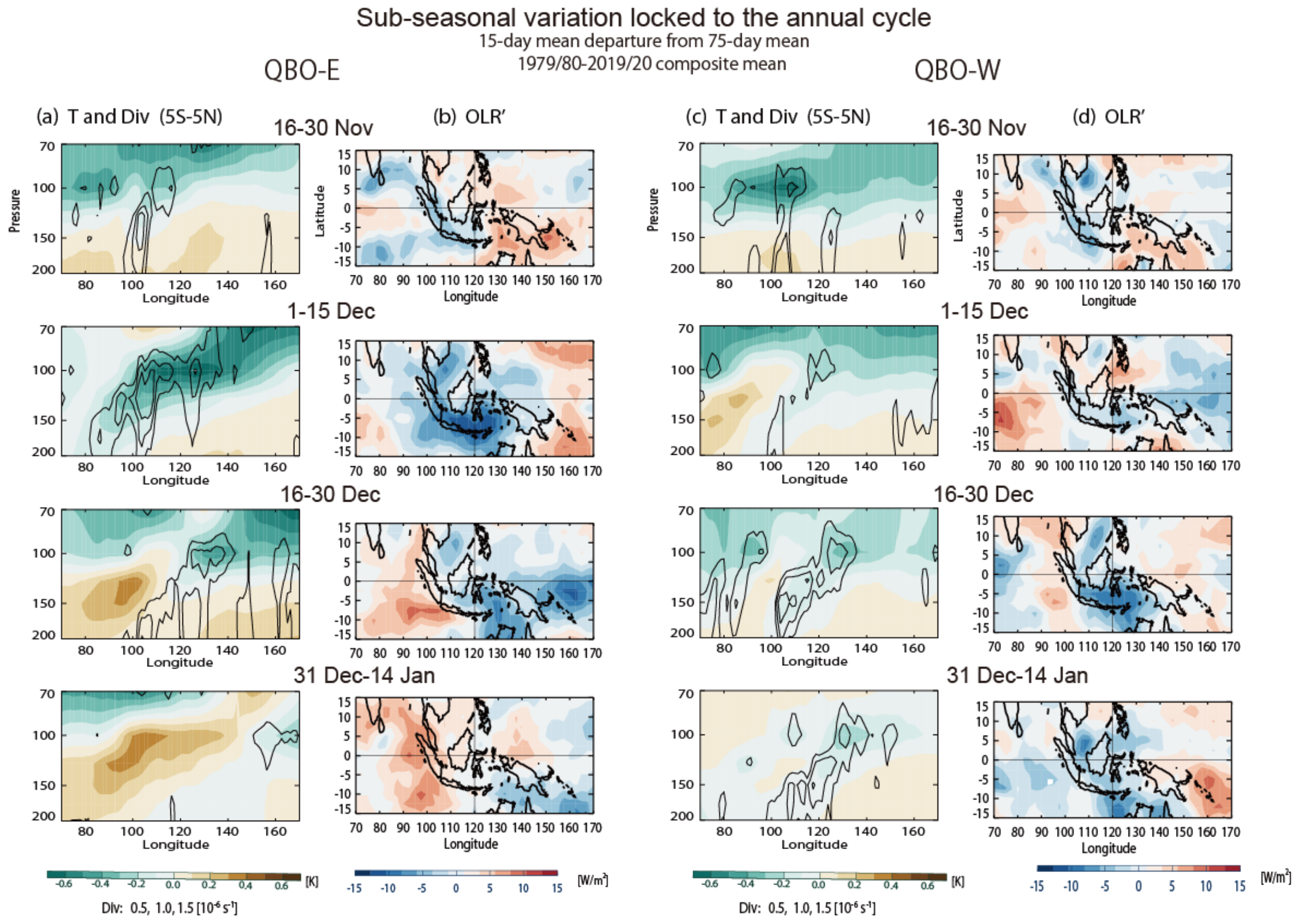

Fig. 6 Composite means of intra-seasonal variation locked to the annual cycle for QBO–E, (a and b) and QBO–W (c and d). Figs. a and c show anomalous temperature (color shadings) and horizontal divergence >0 (contours: 0.5, 1, 1.5 × 10^{-6} s^{-1}), respectively. Figs. b and d shows anomalous OLR. From the top to bottom, 15-day means over 16–30 November, 1–15 December, 16–30 December, and 21 December–14 January.

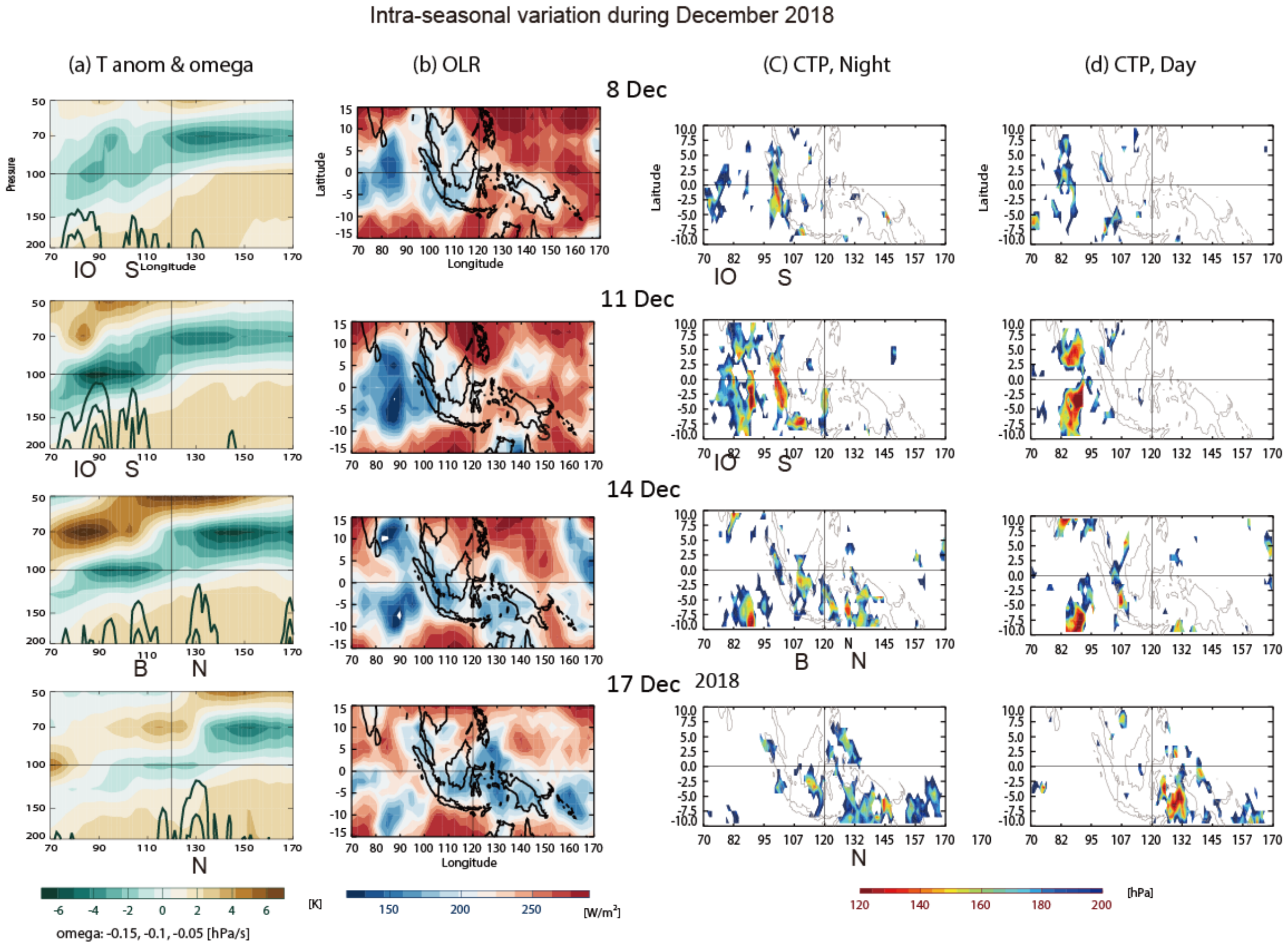

Fig. 7 Intraseasonal component during 2018. (a) Longitude–height cross-sections over the equator (5°S-5°N) for anomalous temperature from climatology (color shading) and pressure vertical velocity < 0 (contours: every −0.05 hPa s^{-1}). (b) OLR. (c) Cloud top pressure from satellite nighttime passes. (d) Same as (c), but from daytime passes. (From top bottom) Consecutive 3-day mean data centered on 8, 11, 14, and 17 December 2018. Letters IO, S, B, N indicate longitudinal position of the Indian Ocean, Sumatra, Borneo, and New Guinea.

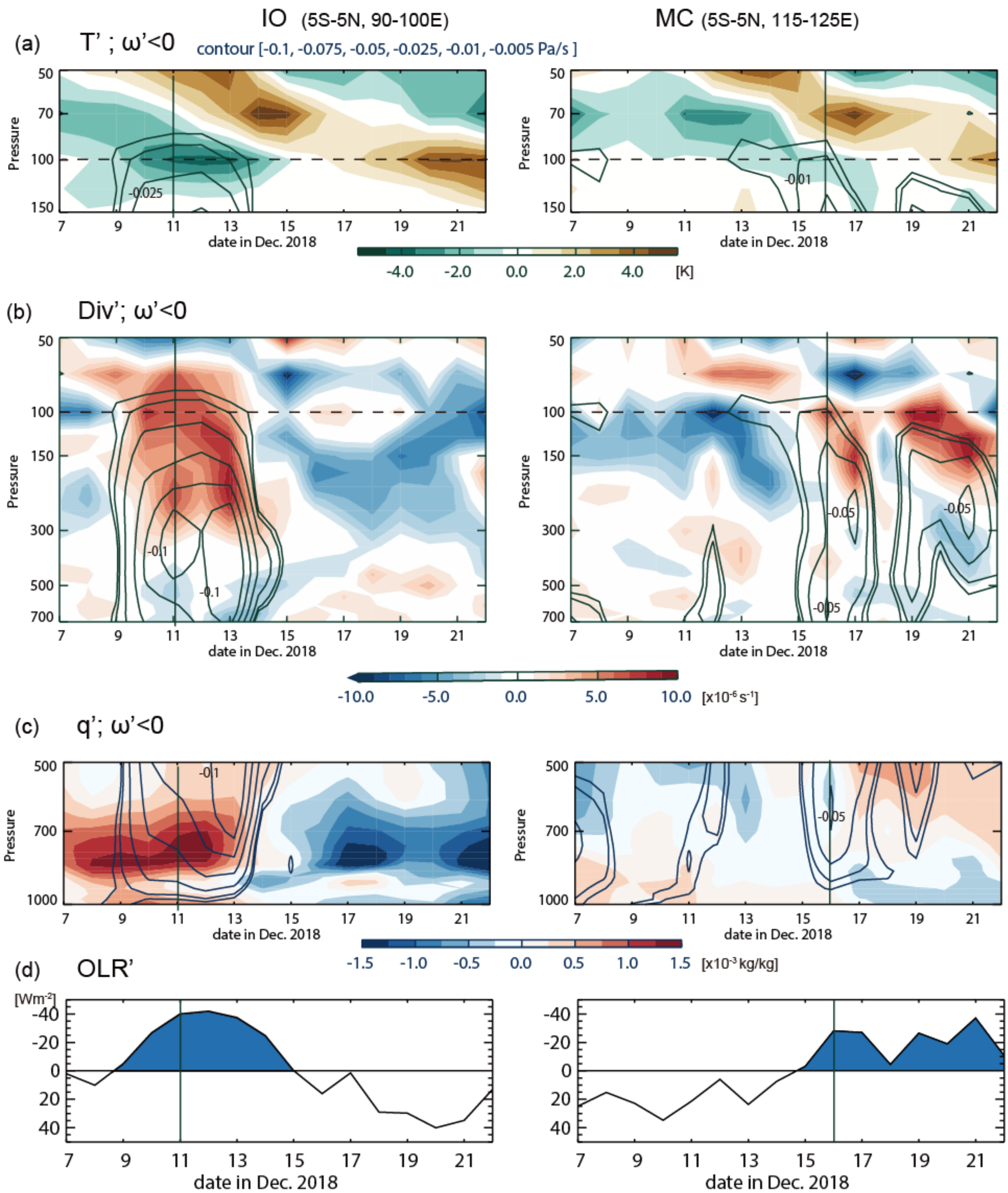

Fig. 8 Time evolution of daily mean data at two locations over the equator (5°S-5°N) over (left) IO (90°-100°E, 5°S-5°N) and (right) MC (115°-125°E, 5°S-5°N). (a-c) Height-time cross-sections of anomalous variables: (a) temperature, (b) horizontal divergence and (c) specific humidity are shown by color shadings, while pressure vertical velocity is shown by contours in a, b, c for ω<0 (-0.1,-0.075, -0.05, -0.025, -0.01, -0.005 hPa s^{-1}). (d) anomalous OLR. Vertical lines indicate the dates 11, and 16 December 2018.

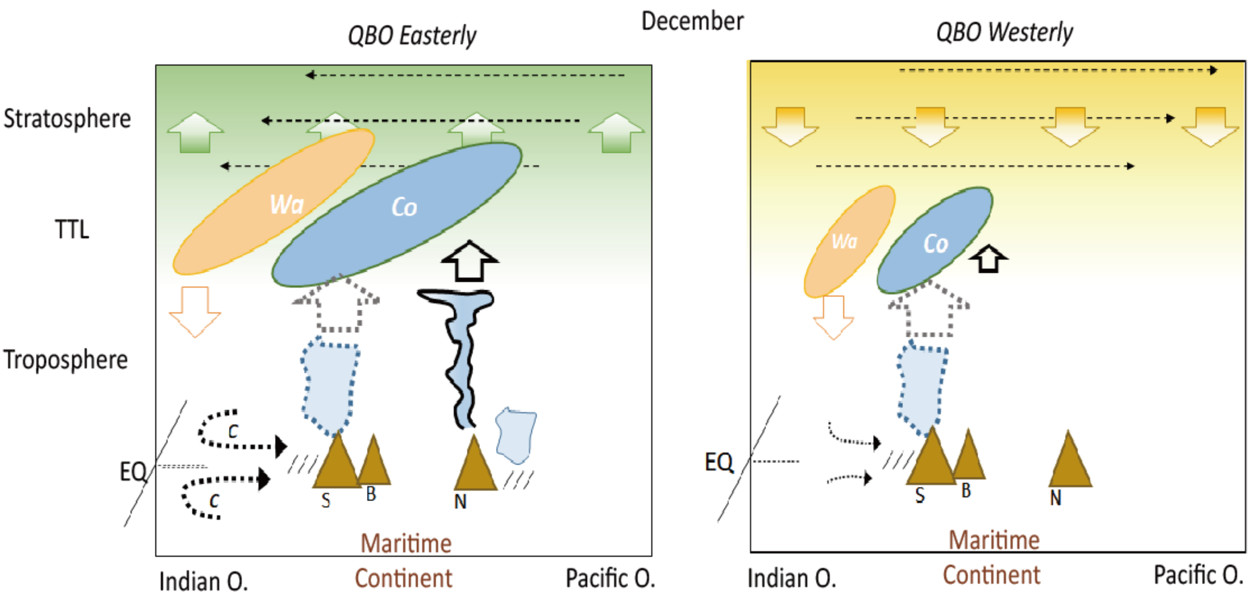

Fig. 9 Schematics of “Kelvin wave bridge” over the Maritime Continent. Letters S, B, N denote Sumatra, Borneo, and New Guinea islands. Wa and Co denote warm and cool anomalies. Arrows indicate vertical and horizontal winds. Cyclonic circulation is noted by c. (See text for more detail).